soft Lewis acids such as BH_3.

The P–N bonds, in **5**, present many interesting features: in contrast to the observations of Songstad et al.[16] and Cowley et al.,[17] there is no linear correlation between the three sums ($\sum N$) of the bond angles around the nitrogen atoms and the three corresponding P–N bond lengths. Figure 2 compares our data with those found by these authors for three triaminophosphane selenides and for $[P(NMe_2)_3]_2Fe(CO)_3$. Like **5**, these four compounds possess three tricoordinated nitrogen atoms bound to a tetracoordinated phosphorus atom. All four display two short P–N bonds (1.65–1.67 Å), with the arrangement of the bonds around the nitrogen being essentially coplanar, and one longer P–N bond (1.68 Å), with the nitrogen atom correlatively adopting a more pyramidal configuration (it should however be noted that this value is still lower than that usually expected for P–N "single" bonds, 1.77 Å[11,20]). In contrast, in **5** it is a short P–N bond (P–N2 = 1.653 (4) Å) that corresponds to the nitrogen having the most pyramidal configuration ($\sum N2 = 341.6 \pm 3.0°$). This is likely to be a consequence of the location of N2 at a bridgehead position between the 5- and 6-membered rings.

This means, as in $Cp(CO)PhFe\overline{P(OCH_2CH_2)_2N}$,[18] where a P–N bond of 1.692 Å has been found, with $\sum N = 333.5°$, that the mechanism responsible for the P–N bond shortening is still effective, in spite of the nonplanar geometry of the N atom. The other two P–N bonds fit better into the correlations of Figure 2: a very short P–N3 bond (1.637 (4) Å) with a planar geometry about N3 ($\sum N = 358.6 \pm 3.0°$) and a long P–N1 bond (1.686 (3) Å) with a more pyramidal nitrogen atom ($\sum N = 348.8 \pm 3.0°$). If one adopts the customarily employed model of Pd_π–N p_π interaction,[19] these data suggest strong p_π–d_π interactions between both N2 and N3 and phosphorus and weaker interactions between N1 and P. Such interactions are of course not the only possible origin of the observed bond shortening; the changing from sp^3 to sp^2 hybridization is also expected to contribute to this shortening.[20]

It should be noticed that N1 has its lone pair approximately trans (dihedral angle of ca. 180°) to the P–B bond and exhibits a smaller sum of bond angles, in accordance both with Songstad's observations and with Cowley's MO calculations for H_2NPH_2[21] and $P(NH_2)_3$,[22] which show that the nitrogen's geometry moves from trigonal planar toward tetrahedral as the dihedral angle increases from 90 to 180°. These considerations encourage us to investigate the basicity of N1 and N2 in **5** toward Lewis acids such as, for example, BF_3.

Figure 1 shows that the diastereoisomer formed is **5′**, the one in which the P–B and N–B bonds are oriented trans to each other with respect to the mean plane of the molecule. In this conformation, the hydrogen atom of the N4–H bond is located in a cavity in the neighborhood of the N1 (2.3 Å) nitrogen atom. The sharp N4HN1 angle (110°) probably hinders[23,24] the formation of a strong hydrogen bond between H(N4) and N1 atoms, and the interaction between the H(N4) and N2 atoms is also impeded by the fact that the free electron pair of N2 is oriented in the opposite direction with respect to the molecule's mean plane.

The six-membered ring adopts the usual low-energy chair conformation and the five-membered ring a slightly flattened "envelope" conformation whose tip is occupied by the phosphorus atom, which can be taken as indicating the absence of particular constraints in the polycyclic structure.

The results presented in this paper are expected to be relevant to most open tautomeric forms of the tetracyclic tetraaminophosphoranes, such as **1a**, **2**, and their homologues and derivatives, whether they are uncomplexed or act as mono- or bidentate ligands toward Lewis acids; different conformations will, however, have to be adopted in the case of chelation.

Registry No. 5′, 84237-92-3.

Supplementary Material Available: Tables of F_o and F_c values, B_{ij} values, hydrogen atom coordinates, and nonessential angles (12 pages). Ordering information is given on any current masthead page.

(16) Romming, C.; Songstad, J. *Acta Chem. Scand., Ser. A* **1979**, *A33*, 187.
(17) Cowley, A. H.; Davis, R. E.; Remadna, K. *Inorg. Chem.* **1981**, *20*, 2146.
(18) Vierling, P.; Riess, J. G.; Grand, A. *J. Am. Chem. Soc.* **1981**, *103*, 2466.
(19) Bach, M. C.; Brian, C.; Crasnier, F.; Labarre, J. F.; Leibovici, C.; Dargelos, A. *J. Mol. Struct.* **1973**, *17*, 23.
(20) Cotton, F. A.; Riess, J. G.; Stults, B. R. *Inorg. Chem.* **1983**, *22*, 133.

(21) Cowley, A. H.; Taylor, M. W.; Whangbo, M.-H.; Wolfe, S. *J. Chem. Soc., Chem. Commun.* **1976**, 838.
(22) Cowley, A. H.; Davis, R. E.; Lattman, M.; McKee, M.; Remadna, K. *J. Am. Chem. Soc.* **1979**, *101*, 5090.
(23) Koetzle, T. E.; Lehmann, M. S. "The Hydrogen Bond-Recent Developments in Theory and Experiments"; Schuster, P., et al., Eds.; North-Holland Publishing Co.: Amsterdam, 1976; pp 459–469.
(24) Olovsson, I.; Jonsson, P. G. In ref 23, pp 400–415, 441–456.

Contribution from the Research School of Chemistry,
Australian National University, Canberra, ACT 2601, Australia

Raman Spectra of Co(NH₃)₆X₃ (X = Cl, Br, I) Complexes

LUCJAN DUBICKI*† and BRYCE WILLIAMSON‡

The vibrational Raman spectra of the complexes $Co(NH_3)_6X_3$ (X = Cl, Br, I) have been measured between 310 and 40 K. The controversial fine structure near 500 cm^{-1} is explained on the basis of inequivalent sites and different isotope shifts for the A_{1g} and T_{1u}^b stretching vibrations. The polarized intensities for the E_g vibration of $Co(NH_3)_6Cl_3$ can be analyzed quantitatively in terms of four inequivalent species. The structure of the iodide complex changes from the high-temperature cubic to a polydomained monoclinic phase near 280 K. Additional structural changes are observed near 250 and 90 K. Off-center displacement in the charge-transfer states of the CoN_6 chromophore may be responsible for the Raman activity of the T_{1u}^b vibration.

1. Introduction

The assignment of the stretching vibrations in $Co(NH_3)_6X_3$ (X = Cl, Br, I) has been a controversial subject for many years.[1–5] Of the two IR-active T_{1u} skeletal modes, the bending

vibration is strong in the IR spectrum but the predominantly stretching vibration (T_{1u}^b) is very weak. The IR bands near

(1) Nakamoto, K.; Morimoto, Y.; Fujita, J. *Proc. Int. Conf. Coord. Chem.* **1962**, *7*, 14–6.
(2) Siebert, H.; Eysel, H. H. *J. Mol. Struct.* **1969**, *4*, 29–40.
(3) Swaddle, T. W.; Craig, P. J.; Boorman, P. M. *Spectrochim. Acta, Part A* **1970**, *22A*, 1559–65 and references therein.
(4) Le Postollec, M. *J. Chim. Phys.* **1975**, *72*, 675–83.

†Visiting Fellow.
‡Present address: Department of Chemistry, University of Virginia, Charlottesville, VA.

Table I. Factor Group (C_{2h}) Analysis for the Stretching Vibrations in $Co(NH_3)_6Cl_3$

	S_1 $2C_2(C_2')$	S_2 $2C_2(C_2')$	S_3 $C_{2h}(C_2')$	S_4 $C_{2h}(C_2')^a$
A_{1g}	A_g, A_u	A_g, A_u	A_g	A_g
E_g	A_g, B_g, A_u, B_u	A_g, B_g, A_u, B_u	A_g, B_g	$2A_g$
T_{1u}	$A_g, 2B_g, A_u, 2B_u$	$A_g, 2B_g, A_u, 2B_u$	$A_u, 2B_u$	$A_u, 2B_u$

^{a} Site symmetry of S_i as given in ref 8. Raman activity: $A_g(XX, YY, ZZ, XY)$, $B_g(ZX, ZY)$.

500 cm^{-1} have been originally assigned to the $T_{1u}{}^b$ vibration, which was assumed to be split in the monoclinic chloride complex.[1] Subsequently Raman spectra showed a strong polarized band at 500 cm^{-1}, and Siebert and Eysel[2] assigned the bands at 500 and 490 cm^{-1} to A_{1g} and $T_{1u}{}^b$ vibrations, respectively. However, Swaddle et al.[3] and Le Postollec[4] suggested the presence of inequivalent sites and assigned both bands to A_{1g}. Other workers[5,6] still maintain that the fine structure may be due to the splittings of the $T_{1u}{}^b$ vibration.

In this paper the problems of octahedral parentage and inequivalency are examined in detail with use of higher resolution and temperature-dependent single-crystal Raman spectroscopy.

2. Experimental Section

2.1. Preparation of Crystals. $Co(NH_3)_6Cl_3$ was prepared by the method of Bjerrum and McReynolds.[7] $Co(NH_3)_6Br_3$ was obtained by passing a solution of the chloride salt through an anion-exchange column with bromide ions occupying the active sites. The less soluble iodide salt was precipitated from a solution of the chloride by the addition of KI. The deuterated complexes were prepared by recrystallization from D_2O. Large crystals of $Co(NH_3)_6Cl_3$, $Co(NH_3)_6I_3$, and $Co(ND_3)_6I_3$ were obtained by slow evaporation in a desiccator.

2.2. Crystal Structure of $Co(NH_3)_6Cl_3$. The space group is $C2/m$, and the factor group is C_{2h}.[8] The monoclinic cell is nonprimitive with two lattice points. Each Bravais cell contains six $Co(NH_3)_6{}^{3+}$ ions situated at the four sites S_1, S_2, S_3, and S_4, which have the Wyckoff notations $2g(C_2)$, $2h(C_2)$, $b(C_{2h})$, and $c(C_{2h})$, respectively. The factor group analysis for the stretching vibrations of the four sites is given in Table I. Each cation has 14 nearest-neighbor chloride ions, eight of which form a distorted cube and six form an irregular octahedron. The hydrogen atoms could not be located.[8]

The site symmetry axis is parallel to the b axis and for S_1, S_2, and S_3 lies along the C_2' axis of the octahedron, i.e. bisecting two Co–N bonds. The S_1 and S_2 octahedra have very small distortions. For example, the axial and effective equatorial Co–N distances for S_1 are 1.970 Å and $1/2(1.974 + 1.963)$ Å = 1.969 Å, respectively. The cubic and octahedral cages of chloride ions are fairly regular with average Co–Cl distances 4.3 and 5.3 Å, respectively. The chloride and metal octahedra have similar orientations. Hence, the species S_1 and S_2 and their outer coordination sphere closely resemble the room-temperature cubic structure of $Co(NH_3)_6I_3$ (see part 2.4).

For S_3, the chloride cages are rotated away from the idealized cubic orientations and the octahedral cage lies closer to the metal ion with an average Co–Cl distance of 4.3 Å. The cubic cage is expanded with Co–Cl distance $\sim$4.9 Å. Both cages are fairly regular, and the S_3 octahedron is only slightly elongated perpendicular to the C_2' axis (Co–N$_{ax}$ = 1.962 Å and Co–N$_{eq}$ = 1.957 Å).

The outer coordination sphere of S_4 resembles S_3, but it is considerably distorted. The chloride octahedra are tetragonally elongated, Co–Cl$_{ax}$ = 6.4 Å and Co–Cl$_{eq}$ = 4.6 Å. The Co–Cl distances for the cubic cage vary between 4.3 and 4.6 Å. The S_4 octahedra are elongated perpendicular to the b axis, which in this case lies along a Co–N bond. The axial bonds (Co–N$_{ax}$ = 1.983 Å) point directly at the axial chloride ions. The equatorial bond lengths, 1.959 and 1.955 Å, show that the in-plane anisotropy is very small.

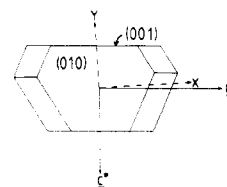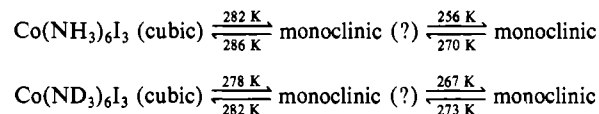**Figure 1.** Crystal morphology of $Co(NH_3)_6Cl_3$. The extinction directions X and Y in the (010) plane for light with $\lambda = 647.1$ nm are rotated by 4° with respect to the a and $\bar{c}^*$ crystal axes. Z is parallel to b.

2.3. Crystal Structure of $Co(NH_3)_6Br_3$. X-ray oscillation and Weissenberg photographs show that the bromide complex has a monoclinic structure.[9] The powder diffraction pattern for $d_{hkl} < 4$ Å corresponds closely to that for the chloride, and single-crystal photographs show no evidence of $h + k = 2n + 1$ reflections. The unit cell is nonprimitive, and the space group is $C2$, C/m, or $C2/m$. The low intensity of reflections above $d_{hkl} = 4$ Å suggests that the structure has no less symmetry than the chloride, and on this basis the space group was assigned $C2/m$ with $a = 12.83$ (1) Å, $b = 21.86$ (1) Å, $c = 13.00$ (1) Å, and $\beta = 112.77$ (2)°.

2.4. Crystal Structure of $Co(NH_3)_6I_3$. At room temperature the iodide complex has the cubic space group $Fm3m$ with $Z = 4$ and $a = 10.52$ Å.[10] The primitive cell contains one regular octahedral cation surrounded by a cubic and an octahedral cage of chloride ions with Co–Cl distances 4.69 and 5.41 Å, respectively. There is no evidence for localized hydrogen positions, and the NH$_3$ groups apparently are "freely" rotating at room temperature. The material displays specific heat anomalies near 282 and 276 K.[11,12] We followed the phase transitions orthoscopically. When the sample was cooled, biaxial domains formed at 282 K (T_1). Many smaller domains appeared at 256 K (T_2). Similar results were obtained for the deuterated complex and are summarized below:

$$Co(NH_3)_6I_3 \text{ (cubic)} \underset{286 \text{ K}}{\overset{282 \text{ K}}{\rightleftharpoons}} \text{monoclinic (?)} \underset{270 \text{ K}}{\overset{256 \text{ K}}{\rightleftharpoons}} \text{monoclinic}$$

$$Co(ND_3)_6I_3 \text{ (cubic)} \underset{282 \text{ K}}{\overset{278 \text{ K}}{\rightleftharpoons}} \text{monoclinic (?)} \underset{273 \text{ K}}{\overset{267 \text{ K}}{\rightleftharpoons}} \text{monoclinic}$$

Borzecka et al.[13] assumed that the low-temperature phase of the iodide salt may be related to the low-temperature phases of Ni(II) and Mg(II) hexaammines. The Raman spectra, however, suggested that the structure may be isomorphous with the room-temperature structure of the chloride complex. In fact, the assumption that the phase below 250 K consists of 12 twinned orientations of a monoclinic unit cell of the chloride type provides a satisfactory indexation of the oscillation photographs.[9]

The temperature dependence of the Raman spectra indicated that all the $Co(ND_3)_6X_3$ salts have the same crystal structure as their protonated analogues.

2.5. Raman Spectroscopy. The Raman equipment has been described elsewhere.[14] All spectra were excited with the 647.1-nm radiation of a Spectra-Physics krypton laser. The samples were cooled in a right-angle circular cross section flow tube. The temperature of the helium gas near the sample was monitored with a gold–chromel thermocouple. Corrections for laser heating were made by comparing the intensity ratio of the Stokes and anti-Stokes scattering. The correction for 100-mW incident power of the 647.1-nm laser line is $\sim$20 K for the ammine complexes of cobalt(III).

Porto notation[15] is used to denote polarizations and scattering geometry. The axes in the laboratory frame are given in the upper case, X, Y, Z, and the molecular axes in the lower case, x, y, z. The Raman spectra of the bending skeletal modes, T_{2g}, $T_{1u}{}^a$, and T_{2u}, were

(5) Schmidt, K. H.; Muller, A. *J. Mol. Struct.* **1974**, *22*, 343–52.
(6) Schmidt, K.; Hauswirth, W.; Muller, A. *J. Chem. Soc., Dalton Trans.* **1975**, 2199–201.
(7) Bjerrum, J.; McReynolds, J. P. *Inorg. Synth.* **1946**, *2*, 217.
(8) Kruger, G. J.; Reynhardt, E. C. *Acta Crystallogr., Sect. B: Struct. Crystallogr. Cryst. Chem.* **1978**, *B34*, 915–7.

(9) Welberry, T. R.; Williamson, B. E. *Acta Crystallogr., Sect. C: Cryst. Struct. Commun.* **1983**, *C39*, 513–4.
(10) Kime, N. E.; Ibers, J. A. *Acta Crystallogr., Sect. B: Struct. Crystallogr. Cryst. Chem.* **1969**, *B25*, 168–9.
(11) Ziegler, W. T. *J. Am. Chem. Soc.* **1941**, *63*, 2700–3.
(12) Goettel, M.; Janik, J. M.; Janik, J. A.; Rachwalska, M. *Phys. Status Solidi A* **1976**, *35*, 675–80.
(13) Borzecka, B.; Hodorowicz, S.; Ciechanowicz-Rutkowska, M. *Acta Phys. Pol. A* **1980**, *A57*, 813–7.
(14) Johnstone, I. W.; Dubicki, L. *J. Phys. C* **1980**, *13*, 121–30.
(15) Damen, T. C.; Porto, S. P. S.; Tell, B. *Phys. Rev.* **1966**, *142*, 570–4.
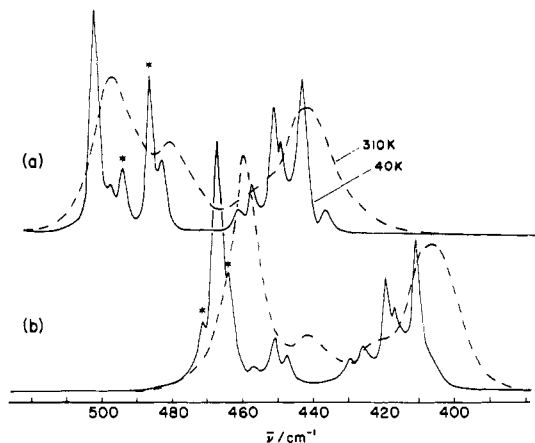
Figure 2. Unpolarized Raman spectra of polycrystalline samples of (a) Co(NH₃)₆Br₃ and (b) Co(ND₃)₆Br₃. The $T_{1u}{}^b$ vibrations are marked by asterisks. For Co(ND₃)₆Br₃, the assignment of $T_{1u}{}^b$ made at 463.5 cm⁻¹ ($\bar{\nu}_H/\bar{\nu}_D = 1.051$) is tentative. It may coincide with the strong band at 466.5 cm⁻¹ ($\bar{\nu}_H/\bar{\nu}_D = 1.044$).

broad and weak. A detailed analysis was not possible, and this work is restricted to the stretching vibrations, A_{1g}, E_g, and $T_{1u}{}^b$.

Crystals of the chloride salt have well-developed (010) and (001) faces. The two extinction directions (X, Y) within the (010) plane are inclined at 4° to the crystal a and $\bar{c}^*$ axes for incident light filtered with a 647.1-nm narrow-band-pass interference filter (Figure 1). The complete set of scattering intensities were obtained from the three configurations $Y()Z$, $X()Z$, and $X()Y$, the last two requiring a polished face in the YZ plane. Crystals of Co(ND₃)₆Cl₃ were small, and only the $Y()Z$ configuration was used.

The morphology of the bromide crystals was similar to that of the chloride. Unfortunately, the crystals were small and of poor optical quality and the Raman measurements were restricted to polycrystalline samples.

The iodide salt crystallized with an octahedral morphology. The trigonal axes X, Y, and Z were chosen to lie along the [1Ī0], [11Ī2], and [111] directions, respectively. The crystals were polished to give the scattering configurations $Y()Z$ and $Y()X$. The Raman scattering was depolarized below 280 K.

3. Results and Discussion

3.1. Octahedral Parentage.
The Raman spectra of the stretching vibrations lie between 510 and 400 cm⁻¹ (Figures 2–6). A one to one correspondence between the fine structures of the protonated and deuterated complexes has been generally assumed,[5] and an isotope shift, $\bar{\nu}_H/\bar{\nu}_D \simeq 1.08$, was obtained for all the stretching vibrations. However, a closer examination of Figures 2–6 shows that a strong band near 485 cm⁻¹ for the protonated complexes is absent in the deuterated analogues. The isotope shift for this band is less than 1.08.

The point mass model[16] and the product rule[17] predict

$$(\bar{\nu}_H/\bar{\nu}_D)_{A_{1g},E_g} = (m_{ND_3}/m_{NH_3})^{1/2} = 1.085 \qquad (1)$$

where m_{NH_3} is the mass of the NH₃ ligand. If the skeletal T_{1u} modes are assumed to be decoupled from the T_{1u} lattice vibrations, the product rule gives

$$(\bar{\nu}_H/\bar{\nu}_D)_{T_{1u}{}^a}(\bar{\nu}_H/\bar{\nu}_D)_{T_{1u}{}^b} = (M_H/M_D)^{1/2}(m_{ND_3}/m_{NH_3}) = 1.116 \quad (2)$$

where M_H is the total mass of the protonated cation. The assignment of the bending mode $T_{1u}{}^a$ is not in dispute, and its isotope shift should be used to predict the isotope shift for $T_{1u}{}^b$. The IR spectra (CsI disk) of the iodide complexes give $\bar{\nu}_H = 315$ cm⁻¹ and $\bar{\nu}_D = 290$ cm⁻¹ for the $T_{1u}{}^a$ band. These numbers and eq 2 predict $(\bar{\nu}_H/\bar{\nu}_D)_{T_{1u}{}^b} = 1.03$. The observed isotope shifts

(16) Shimanouchi, T. *J. Chem. Soc. Jpn.* **1953**, *74*, 266.
(17) Wilson, E. B., Jr.; Decius, J. C.; Cross, P. C. "Molecular Vibrations"; McGraw-Hill: New York, 1955; p 183.

Table II. Relative Raman Intensities for E_g Vibrations in Co(NH₃)₆Cl₃[a]

	$A_g(E_g)$				$B_g(E_g)$	
	I_{XX}	I_{YY}	I_{XY}	I_{ZZ}	I_{ZX}	I_{ZY}
S₁	3.35	0.17	3.24	2	1.41	4.59
S₂	4.05	0.36	2.79	2	1.15	4.85
S₃	0.97	3.94	0.04	1	2.99	0.01
S₄ᵥ	0.24	1.55	0.61	3		
S₄ᵤ	1.34	0.02	1.82	1		

[a] See Appendix for details of calculation.

Table III. Assignment of Stretching Vibrations (cm⁻¹) in Co(NH₃)₆Cl₃ and Co(ND₃)₆Cl₃

310 K		40 K			
$\bar{\nu}_H$	$\bar{\nu}_D$	$\bar{\nu}_H$	$\bar{\nu}_D$	$\bar{\nu}_H/\bar{\nu}_D$	assignt[a]
		506	470	1.077	$A_g(A_{1g})_{1,2,3}$
502	465.5	502	463	1.084	$A_g(A_{1g})_{1,2,3}$
		497.5	475	1.047	$A_g(T_{1u})_{1,2}$
486	464	490	468	1.047	$A_g(T_{1u})_{1,2}$
486	447.5	490	452	1.084	$A_g(A_{1g})_4$
		488	467.5	1.043	$B_g(T_{1u})_{1,2}$
460	425	464	430.5	1.078	$A_g(E_g)_3$
459	425	460	427.5	1.076	$B_g(E_g)_3$
		460	b	b	$A_g(E_g)_4$
457	b	458	b	b	$A_g(E_g)_4$
		454	419	1.084	$A_g(E_g)_{1,2}$
447	423.5	450	415	1.084	$A_g(E_g)_{1,2}$
		446	411	1.085	$A_g(E_g)_{1,2}$
		450	416	1.082	$B_g(E_g)_{1,2}$
442	408	444	410	1.084	$B_g(E_g)_{1,2}$
434	403	439	408.5	1.075	$A_g(E_g)_4$

[a] See text. [b] Appear in polarizations that were not measured for Co(ND₃)₆Cl₃.

lie close to two values, 1.08 and 1.05, for all halide salts. Accordingly the bands with the smaller shift were assigned to $T_{1u}{}^b$ parentage.

3.2. E_g Vibrations in Co(NH₃)₆Cl₃.
The E_g vibrations lie in the 470–460-cm⁻¹ region (Figure 3). The Raman intensities are derived in the Appendix and are listed in Table II. The vibrational energies and assignments are given in Table III, where a band is labeled by the representation of the factor group, the octahedral group, and the site of the cation.

All bands have the same isotope shift, $\bar{\nu}_H/\bar{\nu}_D \approx 1.08$, in agreement with eq 1. The prominent features at 310 K are a B_g band at 442 cm⁻¹ and a A_g band at 447 cm⁻¹. The sum of the intensities for S₁ and S₂ follows the ratios

$$I_{ZY}:I_{ZX}:I_{XX}:I_{XY}:I_{ZZ}:I_{YY} = 9.4:2.6:7.4:6:4:0.5$$

The two bands must be assigned to the overlapping components of $(E_g)_1$ and $(E_g)_2$. Similarly, the A_g band at 460 cm⁻¹ and the B_g band at 459 cm⁻¹ are assigned to $(E_g)_3$. The ZZ intensity and the shoulder in the YY spectrum near 457 cm⁻¹ suggest the presence of a $(E_g)_4$ component. The remaining band at 434 cm⁻¹ must be the second $A_g(E_g)_4$ component. The large splitting, ~20 cm⁻¹, is consistent with the strong tetragonal distortion at the S₄ sites (part 2.2). Both A_g bands are better resolved at 40 K.

The Raman spectra at 40 K do not agree with the predictions of Table I. Reynhardt[18] has suggested that a phase change of the type $C2/m \rightarrow P2/m$ occurs near 170 K. For $P2/m$ symmetry the primitive cell is doubled but the factor and site symmetries remain unchanged. Below 175 K the Raman spectra show line narrowing at 500 and 450 cm⁻¹, but the fine structure is partially resolved only below 100 K. The spectra at 40 K show major splittings for S₁ and S₂, but S₃ and S₄ bands are relatively unaffected. Spectral congestion

(18) Reynhardt, E. C. *J. Magn. Reson.* **1978**, *28*, 441–58.
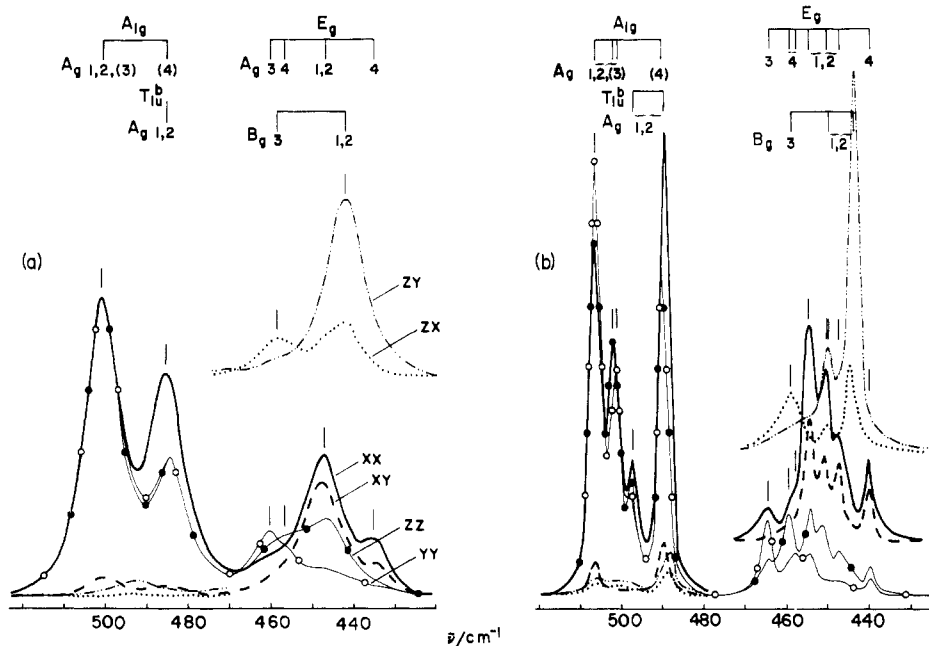
Figure 3. Single-crystal Raman spectra of $Co(NH_3)_6Cl_3$ at (a) 310 and (b) 40 K. The stretching vibrations are classified by the octahedral parentage (A_{1g}, T_{1u}^b, E_g), factor group component (A_g, B_g), and inequivalent site S_i ($i = 1-4$).
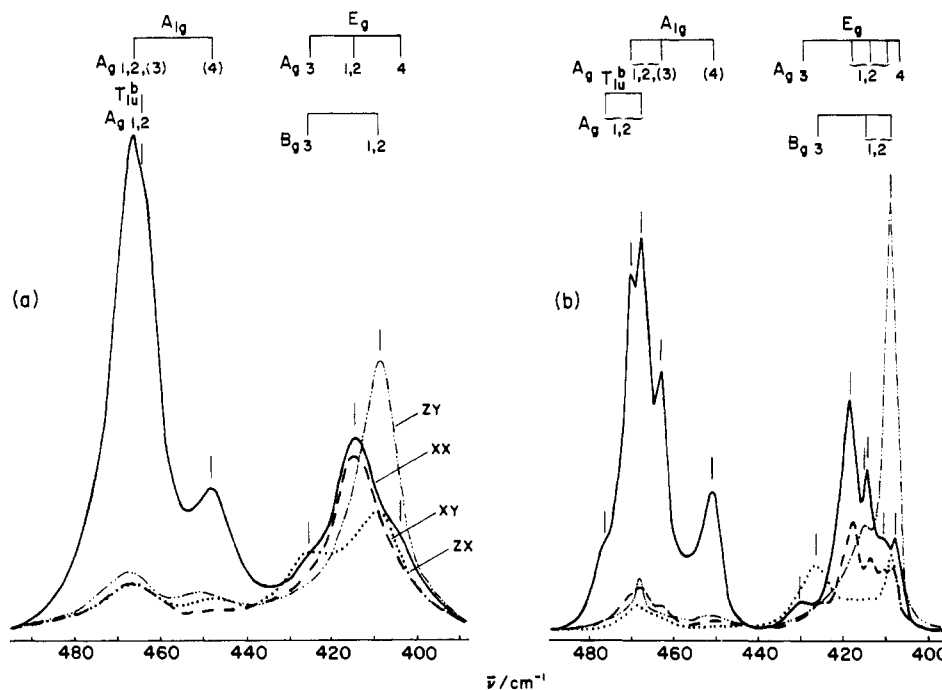

Figure 4. Single-crystal Raman spectra of $Co(ND_3)_6Cl_3$ at (a) 310 and (b) 40 K. The ZZ and YY spectra were not measured (part 2.5). The assignments are the same as in Figure 3.

precludes a detailed analysis, but the fine structure suggests that S_1 and S_2 are converted to three or four new inequivalent species. The distribution of the polarized intensities is consistent with a larger tetragonal distortion perpendicular to the b axis and only a small change in orientation. For example, the ratio I_{ZY}/I_{ZX} remains approximately constant, indicating little change in the tilt angle γ (Appendix). The integrated intensities are similar to the intensities at 310 K and are merely redistributed among the new factor group components. The production of the new and more distorted S_1 and S_2 sites may be responsible for the shoulderlike anomaly in the heat capacity of $Co(NH_3)_6Cl_3$ near 160 K. Clayton et al.[19] have attributed

this anomaly to the restricted motions of the ammonia molecules.

The calculated intensities (Table II) for the S_4 components agree qualitatively with the data at 40 K. Thus the higher energy component, $A_g(E_v)_4$, is more intense in ZZ while the lower energy E_u component is more intense in XX polarization. The theoretical XX and XY intensities are sensitive to the tilt angle γ (Appendix) while the ZZ intensity is very sensitive to the mixing of the u and v components. For example, if we use $\gamma_4 = -26°$, $C_1 = 0.99$, and $C_2 = 0.14$ (Appendix), then the intensity ratios become $I_{XX}:I_{XY}:I_{ZZ}:I_{YY} = 0.28:0.26:3.44:1.76$ and $1.86:1.60:0.56:0.38$ for the v and u components, respectively. Experimental error as well as small changes in orientation that may be associated with the phase transition probably account for most of the discrepancy with

(19) Clayton, P. R.; Staveley, L. A. K.; Weir, R. D. *J. Chem. Phys.* **1981**, 75, 5464–73.
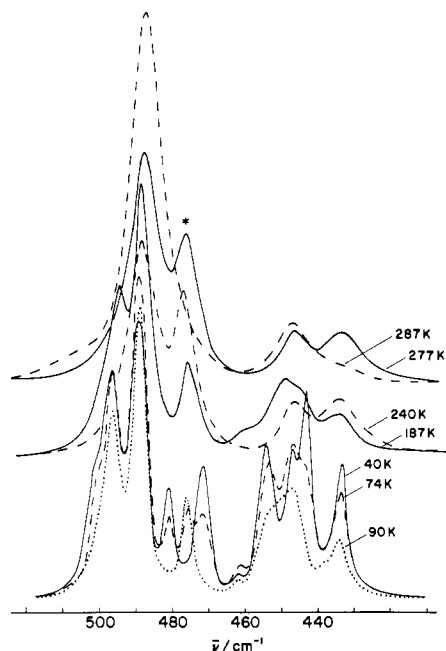
Figure 5. Temperature dependence of the *XX* Raman spectrum of Co(NH₃)₆I₃ between 287 and 40 K. The cubic → monoclinic transition occurs in two stages, 282 K (T_1) and 256 K (T_2), on cooling (part 2.4). A third transition is observed at 90 K (T_3). The asterisk denotes the T_{1u}^b and $(A_{1g})_4$ vibrations (see text). The spectra are depolarized below T_1.
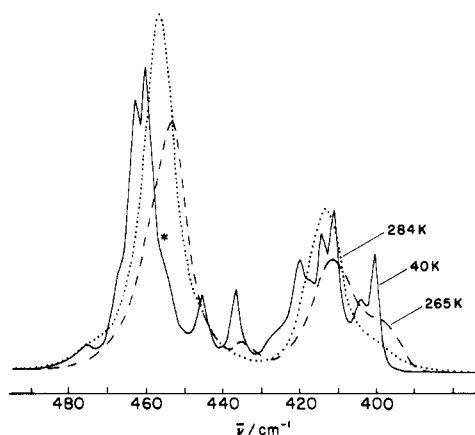
Figure 6. Unpolarized single-crystal $Y(\ )Z$ Raman spectra of Co-(ND₃)₆I₃. The intensity of the T_{1u}^b band, denoted by an asterisk, decreases below 80 K (T_3).

theory. We conclude that the octahedral site approximation (Appendix) is accurate even for the strongly distorted S_4 sites.

3.3. A_{1g} Vibrations in Co(NH₃)₆Cl₃. The A_{1g} scattering tensors are invariant to rotation, and $I_{XX} = I_{YY} = I_{ZZ}$ is predicted for the four sites. This relationship is followed for the band at 502 cm⁻¹ in the 310 K spectrum (Figure 3). The intensities $I_{XX} \simeq 2I_{YY} = 2I_{ZZ}$ as well as deuteration shifts (Table III) for the band at 486 cm⁻¹ indicate the presence of both T_{1u}^b and A_{1g} vibrations. Since the A_{1g} bands of S_1 and S_2 contribute twice the intensity of the corresponding S_3 and S_4 species (Appendix), the band at 502 cm⁻¹ must involve $A_g(A_{1g})_{1,2}$. The *YY* (=*ZZ*) intensities of the 486-cm⁻¹ band are about one-third those of the 502-cm⁻¹ band. Some of this intensity may be due to $A_g(T_{1u}^b)$, and the octahedral site approximation (part 3.2) requires that either $(A_{1g})_3$ or $(A_{1g})_4$ lies at 486 cm⁻¹. Comparison with the unambiguous assignments for the E_g vibration (part 3.2) suggests that $(A_{1g})_4$ may lie at lower energy, and we assign the 486-cm⁻¹ band to A_g-$(A_{1g})_4 + A_g(T_{1u})_{1,2}$ and the 502-cm⁻¹ band to $A_g(A_{1g})_{1,2,3}$.

The polarized spectra at 40 K show fine structure that resembles the splittings in the E_g region. The phase change near 170 K (part 3.2) removes the near-degeneracy of S_1 and S_2. The weak band at 497.5 cm⁻¹ is tentatively assigned to a new $A_g(T_{1u}^b)$ component on the basis of the apparent deuteration shift (Figure 4 and Table III).

3.4. T_{1u}^b Vibration in Co(NH₃)₆Cl₃. According to Table I the allowed $A_g(T_{1u})$ vibrations must belong to the S_1 and S_2 species. The B_g components are very weak and may lie at 488 cm⁻¹ in the 40 K spectrum. The splitting of the T_{1u} vibration appears to be very small, a fact consistent with the small distortions of S_1 and S_2 (parts 2.2 and 3.2). The analysis of the bands at 486 and 502 cm⁻¹ (part 3.3) implies that most of the *YY* and *ZZ* intensity at 486 cm⁻¹ is due to $(A_{1g})_4$ and that the coincident $A_g(T_{1u})$ component has $I_{XX} \gg I_{YY} = I_{ZZ}$. The large intensity of $A_g(T_{1u})_{1,2}$ is rather surprising and merits further comment.

Normal-coordinate analysis of the cubic unit cell of Co(N-H₃)₆I₃ gives significant external interaction force constants between the halide of the cubic cage and the NH₃ groups.[20] Hydrogen bonding (N-H···X) may play an important role in the cubic → monoclinic phase transition of the trihalide complexes. The hydrogen bonding should be increased if the cobalt ion is excited into the charge-transfer state $^1T_{1u} \leftarrow {}^1A_{1g}$ ($e_g \leftarrow \sigma, \pi t_{1u}$) where one electron is formally transferred from the six NH₃ groups to the metal e_g orbital. The $^1T_{1u} \leftarrow {}^1A_{1g}$ transition is very intense, $\epsilon_m > 20\,000$ and $\bar{\nu} = 47\,600$ cm⁻¹ for Co(en)₃³⁺,[21] and should be an important intermediate state in a Frank–Condon scattering mechanism.[22] We suggest that the intensity of the $A_g(T_{1u})$ band is due to "near-resonance" Raman scattering involving an off-center displacement in the intermediate state. The intensity relationship $I_{XX} \gg I_{YY} = I_{ZZ} \simeq 0$ requires the displacement in the Z' (parallel to b axis) component of the $^1T_{1u}$ state to be very small.

3.5. Stretching Vibrations in Co(NH₃)₆I₃. The single-crystal Raman spectra at 310 K follow the octahedral selection rules $I_{XX} = I_{YY} = I_{ZZ}$ for A_{1g} and $I_{XZ} = I_{YZ} = 2I_{XX} = 2I_{XY}$ and $I_{ZZ} = 0$ for E_g vibrations, where X, Y, and Z are the crystal axes which match with the trigonal axes of the cation.

The temperature dependence of the spectra is shown in Figure 5 and 6. The phase change at 282 K (T_1) is associated with new bands at 477 and 435 cm⁻¹, which are assigned to $(T_{1u}^b)_{1,2} + (A_{1g})_4$ and $(E_g)_4$, respectively. For the deuterated complex (Figure 6) the T_{1u}^b band overlaps with $(A_{1g})_{1,2,3}$ and $(A_{1g})_4$ occur as a weak band at 435 cm⁻¹, in agreement with the predicted isotope shifts (part 3.1). The domain formation (part 2.4) depolarizes the incident and scattered radiation, resulting in a sharp decrease in the intensity of the A_{1g} band at 489 cm⁻¹.

Below 240 K new bands appear at 495 and 460 cm⁻¹, indicating distortion and removal of the near-degeneracy of S_1, S_2, and S_3 sites. These structural changes may correspond to the phase transition observed in Co(NH₃)₆Cl₃ at 170 K (part 3.2). The sharp onset of the 495-cm⁻¹ band does not appear to correlate with the second phase transition, which was observed orthoscopically at $T_2 = 256$ K (part 2.4).

A third structural change occurs at $T_3 \approx 90$ K for the protonated and ∼80 K for the deuterated complex. The T_{1u}^b band becomes very weak, and new bands appear at 502, 482, and 472 cm⁻¹. The last two correspond to a sharp increase in the intensity at 433 and 443 cm⁻¹. The same behavior is observed in Co(ND₃)₆I₃, where the T_{1u}^b band overlaps with the A_{1g} bands, but there is a marked decrease in the intensity

(20) Del Rey, M.; Hase, Y. *An. Acad. Bras. Cienc.* **1979**, *51*, 87–92.
(21) Stein, P.; Miskowski, V.; Woodraff, W. .; Griffin, J. P.; Werner, K. G.; Gaber, B. P.; Spiro, T. G. *J. Chem. Phys.* **1976**, *64*, 2159–67.
(22) Tang, J.; Albrecht, A. C. "Raman Spectroscopy"; Szymanski, H. A., Ed.; Plenum Press: New York, 1970; pp 33–68.

at 455 cm^{-1} (Figure 6). It is clear that S_4 is replaced by the two new sites. The disappearance of the $T_{1u}{}^b$ band that is associated with S_1 and S_2 is a puzzle. There are a number of possible explanations, but without polarization data we prefer not to speculate.

4. Conclusions

Previous difficulties in the analysis of the stretching vibrations in $Co(NH_3)_6X_3$ are essentially resolved. The fine structure is due to inequivalent species. The deuterium shifts are explained by the point mass approximation and the Redlich–Teller product rule. The polarized Raman intensities for the A_{1g} and E_g vibrations are accurately predicted by the octahedral site model. Off-center displacement in the charge-transfer states may account for the large scattering intensity of the $A_g(T_{1u}{}^b)$ vibration.

A detailed analysis of the Raman fine structure was not possible for the polydomained iodide complex. Single-crystal spectra of the bromide complex would be a useful extension of this work. The spectra of the bromide (Figure 2) match very closely the average of the polarized spectra of the chloride complex (Figures 3 and 4). However, the bromide does have more than one type of S_4 species, as is also observed in the iodide complex.

The Raman spectra were not useful in analyzing the dynamics of cation reorientations.[18,23] Although line narrowing resulting from the loss of dynamic disorder was observed in many cases, the dominant feature is lattice relaxation, which produces many inequivalent sites. The spectral congestion vitiated an accurate study of the line shapes. The Raman spectra show clearly that the magnitude and direction of the tetragonal distrotion at the S_4 site in $Co(NH_3)_6Cl_3$ remains unchanged from 310 to 40 K (part 3.2). Isotropic reorientations[23] of S_4 are unlikely to occur at room temperature.

Appendix: E_g Scattering Tensors for Inequivalent Sites in $Co(NH_3)_6Cl_3$

The Euler angles[24] $\alpha(z)$, $\beta(y')$, and $\gamma(z'')$ required to transform the cubic axes of the cation octahedra to the crystal extinction directions X, Y, and Z may be obtained from the crystallographic data.[8,18] A near-octahedral molecule with a C_2 symmetry axis bisecting two bonds has an effective tetragonal symmetry perpendicular to the C_2 axis. Choosing z to lie perpendicular to C_2 ensures that the real components of the octahedral E representation split diagonally into the irreducible representations of the C_2 or C_{2h} site group. Linear combinations of the bases for the two equivalent molecules in the primitive cell then give the gerade and ungerade factor group representations (Table I). For S_4 the C_2 axis lies along the Co–N bond, and in this case the choice of z axis is arbitrary. However, if the z axis lies along the direction of tetragonal distortion, then the tetragonal contributions to the splitting of the E_g vibrations are diagonal. Hence for all species

the z axis is chosen to lie perpendicular to the C_2 (b) axis. The b axis bisects the x and y axes for S_1, S_2, and S_3 and coincides with x for S_4. This choice of cubic axes gives $\alpha_i = -135°$ and $\beta_i = -90°$ ($i = 1$–3), $\gamma_1 = -29°$, $\gamma_2 = -26°$, $\gamma_3 = -86°$, $\alpha_4 = 180°$, $\beta_4 = -90°$, and $\gamma_4 = -32°$.

In the octahedral site approximation the scattering tensor in the cubic frame (x, y, z) is taken to be the octahedral scattering tensor, $\mathbf{P}_{\alpha\beta}$. The tensor in the laboratory frame (X, Y, Z) for species S_i is given by

$$[\mathbf{P}_{\rho\sigma}]_i = R_i[\mathbf{P}_{\alpha\beta}]R_i^{-1}$$

where $[X] = R[x]$. The diagonal A_{1g} tensor is independent of orientation. The octahedral tensors for E_g vibrations are

$$E_u: \quad a_2 \begin{bmatrix} -1 & \cdot & \cdot \\ \cdot & -1 & \cdot \\ \cdot & \cdot & 2 \end{bmatrix} \qquad E_v: \quad 3^{1/2}a_2 \begin{bmatrix} 1 & \cdot & \cdot \\ \cdot & -1 & \cdot \\ \cdot & \cdot & \cdot \end{bmatrix}$$

where a_2 is a constant. For S_1, S_2, and S_3, E_u and E_v transform as the A and B representations in the C_2 or C_{2h} site group. The scattering tensors in the laboratory frame are

$$A_g(E_u)_i: \quad a_2 \begin{bmatrix} 2 - 3\sin^2\gamma_i & -3/2\sin 2\gamma_i & \cdot \\ -3/2\sin 2\gamma_i & 2 - 3\cos^2\gamma_i & \cdot \\ \cdot & \cdot & -1 \end{bmatrix}$$

$$B_g(E_v)_i: \quad 3^{1/2}a_2 \begin{bmatrix} \cdot & \cdot & \sin\gamma_i \\ \cdot & \cdot & \cos\gamma_i \\ \sin\gamma_i & \cos\gamma_i & \cdot \end{bmatrix}$$

$$A_g(E_u)_4: \quad a_2 \begin{bmatrix} 3\cos^2\gamma_4 - 1 & -3/2\sin 2\gamma_4 & \cdot \\ -3/2\sin 2\gamma_4 & 3\sin^2\gamma_4 - 1 & \cdot \\ \cdot & \cdot & -1 \end{bmatrix}$$

$$A_g(E_v)_4: \quad 3^{1/2}a_2 \begin{bmatrix} -\sin^2\gamma_4 & -1/2\sin 2\gamma_4 & \cdot \\ -1/2\sin 2\gamma_4 & -\cos^2\gamma_4 & \cdot \\ \cdot & \cdot & 1 \end{bmatrix}$$

where $i = 1$–3. The vibrational wave functions for components of $(E_g)_4$ can couple, viz.

$$(E_+) = C_1(E_v) - C_2(E_u)$$

$$(E_-) = C_2(E_v) + C_1(E_u)$$

and the corresponding tensors are linear combinations of the two A_g tensors. The scattering intensities are given by

$$I_{\sigma\rho_i} \propto g_i|\mathbf{P}_{\rho\sigma_i}|^2$$

where g_i is the multiplicity of S_i in the primitive cell, $g_1 = g_2 = 2$, and $g_3 = g_4 = 1$. The relative intensities are given in Table II.

(23) Reynhardt, E. C.; Lourens, J. A. J.; Smit, E. *J. Magn. Reson.* **1979**, *33*, 303–10.

(24) Messiah, A. "Quantum Mechanics"; North-Holland Publishing Co.: Amsterdam, 1970; Vol. 2, p 1068.